Geosynthetics, J. Kuwano & J. Koseki (eds)

Viscous property and time-dependent degradation of geosynthetic reinforcement

Tatsuoka, F., Kongkitkul, W. & Hirakawa, D.
Department of Civil Engineering, Tokyo University of Science, 2641 Yamazaki, Noda, Chiba 278-8510, Japan

Keywords: viscous property, polymer, geosynthetic, geogrid, reinforcement

ABSTRACT: The viscous property, which causes creep deformation, of polymer geosynthetic reinforcement is reviewed. The creep deformations and associated creep rupture strengths when subjected to long-term sustained loading either with simultaneous degradation or after degradation that has taken place for full life time (i.e., the current design method) are simulated and compared. It is shown that the current design method that evaluates the long-term tensile design strength by separately applying reduction factors for creep rupture and degradation may largely under-estimate the creep rupture strength at the end of service time.

1 INTRODUCTION

Currently, the long-term tensile design strength (i.e., the design applied load), T_d, of a given geosynthetic reinforcement is obtained by separately accounting for the effects of creep deformation and degradation, typically as Eq. 1 (FHWA, 2001):

$$T_d = \frac{T_{\text{ult}}}{RR_{CR} \cdot RF_D \cdot RF_{ID} \cdot (F_s)_{\text{overall}}} \quad (1)$$

where T_{ult} is the tensile strength based on minimum average role value by tensile tests at a specified strain rate; RF_{CR} is the creep reduction factor to avoid creep rupture until the end of service life; RF_D is the durability reduction factor (typically 1.1–2.0) to account for long term chemical and/or biological degradation effects; RF_{ID} is the installation damage factor (typically 1.05–3.0); and $(F_s)_{\text{overall}}$ is the overall safety factor (usually > 1.5) to account for uncertainties in the design parameters. This procedure is represented by steps 1–5 in Fig. 1. The value of RF_{CR} is obtained from a given creep-rupture curve (Fig. 1), which is different among different geosynthetic types and different countries: e.g., 4.0 – 5.0 for PP & 2.6–5.0 for HDPE in FHWA (2001). The creep rupture curve is not a diagram of reduction in strength against time, even though this may appear to be so. In fact, without degradation, the initial strength evaluated at a given strain rate is maintained until late in its service life (Greenwood et al., 2001; Tatsuoka et al., 2004). Moreover, Eq. 1 assumes that long-term sustained loading starts after the material has fully degraded by a factor of $1/RF_D$ by the use in the backfill for service life (i.e., after having backed from the future). In actuality, however, creep deformation and degradation take place simultaneously.

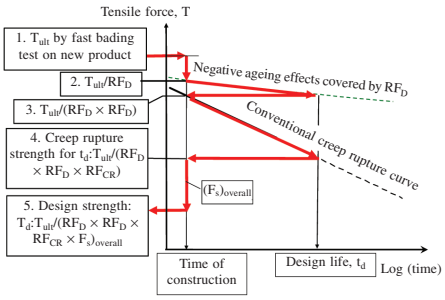

Figure 1. FHWA procedure to determine the design stength.

In this study, creep rupture strengths when degradation takes place during sustained loading (SL) and when SL starts after full degradation for service life has taken place (i.e., Eq. 1) were numerically simulated by introducing degradation effects into a non-linear three-component model (Fig. 2) and compared. According to this model, given tensile load,

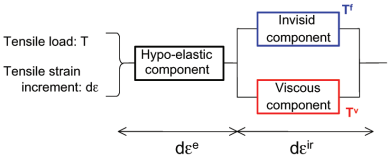

Figure 2. Non-linear three-component rheology model for geosynthetic reinforcement (Hirakawa et al., 2002).

T, consists of inviscid and viscous components, T^f and T^v, while a given strain increment, $d\varepsilon$, consists of elastic and in-elastic (or irreversible or visco-plastic) components, $d\varepsilon^e$ and $d\varepsilon^{ir}$. During SL at a fixed load, T, T^v decreases and the creep strain, $\Delta\varepsilon^{ir}$, increases with time. The degradation is another time-dependent phenomenon, by which the creep rupture curve drops with time.

2 VISCOUS PROPERTY

The viscous property of polymer geosynthetic reinforcement can be quantified by stepwise changing the strain rate many times during otherwise monotonic loading (ML) at a constant strain rate (Fig. 3a). It is assumed in Fig. 3a that the current tensile load, T, is a unique function of instantaneous irreversible strain, ε^{ir} and its rate $\dot{\varepsilon}^{ir}$. This property is called the isotach viscosity and relevant to most polymer geosynthetic reinforcements tested by Hirakawa et al. (2003). They divided the load jump, ΔT, observed upon the respective step change in the strain by the instantaneous load, T, and plotted against the logarithm of the ratio of the $\dot{\varepsilon}^{ir}$ values after and before a step change (Fig. 3b). For the data presented in Fig. 3b, only PET yarn

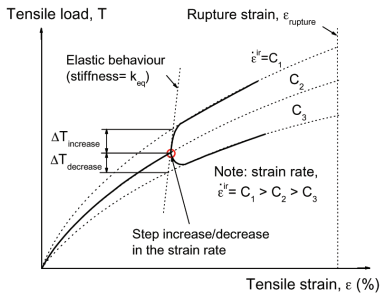

Figure 3. (a) Method to quantify the viscous property.

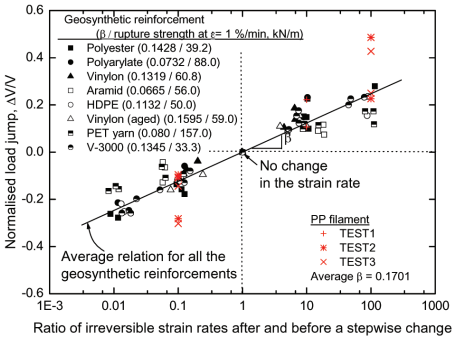

Figure 3. (b) Rate-sensitivity coefficients of polymer geosynthetic reinforcements (Hirakawa et al., 2003; Kongkitkul, 2004) and PP filament (Fig. 5).

is part of a geocomposite while the others are all geogrids. The data of polypropylene (PP) filament are described below. The slope of the linear relation fitted to the respective test data is defined as the rate-sensitivity coefficient, β (Tatsuoka, 2004; Di Benedetto et al., 2005). The values of β and rupture strengths of the tested materials are listed in Fig. 3b. It may be seen that the range of these β values is relatively small.

The β values of different polymer geosynthetic reinforcements were also obtained from the data of continuous ML tests at different strain rates found in the literature (e.g., Fig. 4). Tensile loads (T) at the same strain (ε) were read from $T-\varepsilon$ curves for different strain rates. Assuming the isotach viscosity, the difference in the tensile loads, ΔT, at two different strain rates (e.g., C_1 & C_2 in Fig. 3a) was taken to be equivalent to the load jump upon a strain rate jump from C_2 to C_1. Table 1 summarises the β values thus obtained, which are of the same order as those listed in Fig. 3b. However, the β values from different experiments of the respective same geogrid type are noticeably different. It seems that the viscous property could be somehow different among different products of the same geogrid type.

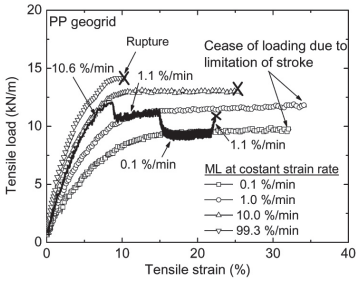

Figure 4. Rate-dependent $T-\varepsilon$ relattions of PP geogrid (Shinoda et al., 2002; Shinoda & Bathurst, 2004).

Table 1. β values from data found in the literature.

Reinforcement type	Range of strain rate (%/min)	Viscosity: β	References
HDPE	0.2 – 20 (0.2, 1, 10, 20)	0.2256	Hirai and Yatsu (2000)
HDPE	1 – 300 (1, 10, 60, 300)	0.3336	Bhathurst and Cai (1994)
HDPE	0.1 – 98.1 (0.1, 1, 10.1, 98.1)	0.2524	Shinoda et al. (2002)
PET	1 – 125 (1, 10, 125)	0.1272	Bathurst and Cai (1994)
PP	0.1 – 99.3 (0.1, 1, 10, 99.3)	0.2326	Shinoda et al. (2002)

Figure 5 shows the $T-\varepsilon$ relations from tensile tests on single polypropylene (PP) filaments in which the strain rate was stepwise changed during otherwise

ML. The trend of rate-dependency seen from Fig. 5 and the β value, shown in Fig. 3b, of single PP filament are similar to those of PP geogrid (Figs. 3b & 4). This result indicates that the viscous property of polymer geosynthetic reinforcement is due mostly to the viscous property of the constituting material.

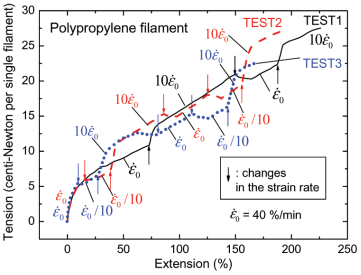

Figure 5. Rate-dependent T - ε relations of PP filament.

3 DEGRADATION DURING CREEP

Tatsuoka et al. (2003) modified the model (Fig. 2) to account for the ageing effects by introducing the inviscid yield stress, $(T_f)_y$, that changes with time. It was assumed that $(T_f)_y$ at a given ε^{ir} decreases with an increase in the elapsed time t_c since the start of degradation by a factor of $A^f(t_c)$ presented in Fig. 6. Yield takes place only when $T_f = (T^f)_y$ and $dT^f = d(T^f)_y$ are satisfied. β = 0.113, which does not to change with time, was assumed.

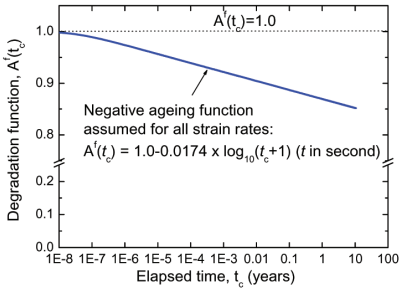

Figure 6. Degradation function assumed in the simulation.

Figure 7a shows the T–ε relations obtained by numerical simulation of ML tests followed by a SL stage. Figure 7b shows the creep strains when T = 32 kN/m plotted against the elapsed time since the start of SL obtained from the simulations in the following three cases: *case 1:* the T–ε property does not degrade with time; *case 2:* ML starts after the T–ε property has degraded at V = 0 for full service life (10 years in the present case) with no degradation after ML starts (i.e., Eq. 1); and *case 3:* degradation starts at the start of sustained loading (SL) and continues during subsequent SL as in actual field cases. The effects of degradation during ML until the start of SL, if taken

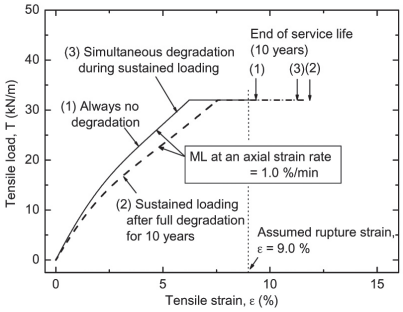

Figure 7. (a) T – ε relations under three degradation conditions.

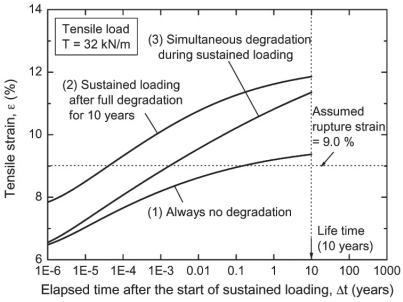

Figure 7. (b) Time histories of creep strain in three cases.

into account, are negligible. The creep strain at the end of service life in case 3 is much larger than in case 1 due to continuous degradation during SL, while it is consistently smaller than case 2.

Figure 8 shows the simulated T – ε relations when ML is followed by SL that continues for 10 years at different tensile loads in case 3. With all the geosynthetic reinforcements tested by Hirakawa et al. (2003), the strain at tensile rupture was essentially independent of loading period until rupture. In the present study, a rupture strain of 9% was assumed. The conclusions from this study do not change by changes in this rupture strain. From Fig. 8 and similar ones for cases 1 and 2, the elapsed time when creep rupture takes place (i.e., when ε becomes 9%) since

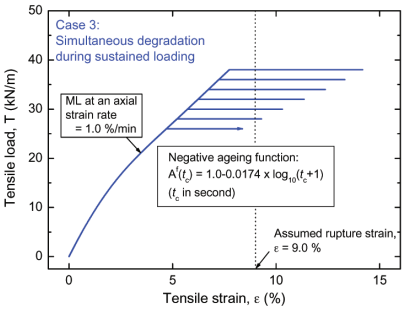

Figure 8. Numerical simulation of creep rupture in case 3.

the start of SL was obtained for the respective sustained load. Figure 9 compares the relationships between the sustained load and the creep rupture time (i.e., the creep rupture curves) for the three cases. The creep rupture strength in case 3 becomes smaller to a larger extent with time than case 1. On the other hand, the creep rupture strength in case 2 is consistently smaller than case 1, while a noticeable difference between cases 2 & 3 remains even at the end of service life. This result indicates that case 2 (i.e., Eq. 1) more-or-less underestimates the creep rupture strength at the end of service life.

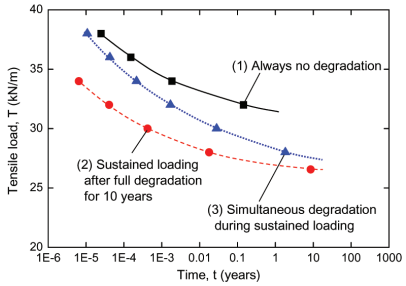

Figure 9. Creep rupture curves in three cases.

Tatsuoka et al. (2004) proposed to remove the creep reduction factor RF_{CR} from Eq. 1 by following steps 1–5 illustrated in Fig. 10. That is, for a given tensile strength, T_{ult}, the design tensile strength under static and seismic loading conditions, $(T_d)_{static}$ and $(T_d)_{seismic}$ (i.e., T_d in Fig. 10), are determined as:

$$(T_d)_{static} = T_{ult}/\{RF_D \cdot RF_{ID} \cdot (F_s)_{overall.static}\} \quad (2a)$$

$$(T_d)_{seismic} = T_{ult}/\{RF_D \cdot RF_{ID} \cdot (F_s)_{overall.seismic}\} \quad (2b)$$

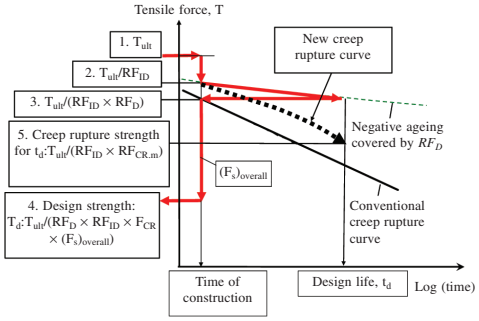

Figure 10. Design strength not controlled by creep rupture.

Here, a difference between the strain rates under static and seismic loading conditions may be accounted for. These values of $(T_d)_{static}$ and $(T_d)_{seismic}$ are equal to the design static and seismic working loads obtained by relevant stability analysis with F_s = 1.0. For conservatism, the residual angle of friction is used as the design shear strength in the static design, while, in the seismic design, the peak shear strength is used to locate the critical failure plane and the limit equilibrium is evaluated by using the residual shear strength (Tatsuoka et al., 1998). $(T_d)_{seismic}$ is usually larger than $(T_d)_{static}$. Finally, it is confirmed that the design static load, $(T_d)_{static}$, is smaller than the creep rupture strength obtained as $T_{ult}/\{RF_{CR.m} \cdot RF_{ID}\}$. Here, $RF_{CR.m}$ is the modified creep reduction factor accounting for simultaneous degradation (case 3), based on the new creep rupture curve in Fig. 10 determined by numerical simulation for given conventional rupture curve and degradation function (Fig. 6), as shown in this paper.

4 CONCLUSIONS

It is shown that the current method to obtain the long-term design tensile strength of geosynthetic reinforcement by separately accounting for the effects of creep deformation and degradation under-estimates the true creep rupture strength, likely largely in many cases. It is suggested to determine the long-term design tensile strength without using a creep reduction factor, in particular in seismic zones.

ACKNOWLEDGEMENTS

The authors acknowledge Dipl. Ing. Gernot Mannsbart, Polyfelt GmbH, Austria, for allowing them to use the test data of PP filament. The financial support from the Japanese Society for the Promotion of Science is deeply appreciated.

REFERENCES

Bathurst, R.J. and Cai, Z. (1994). "In-isolation cyclic load-extension behavior of two geogrids", *Geosynthetics International*, 1 (1): 3-17.

Di Benedetto, H., Tatsuoka, F., Lo Presti, D., Sauzéat, C. and Geoffroy, H. (2005). "Time effects on the behaviour of geomaterials", *Deformation Characteristics of Geomaterials: Recent Investigations and Prospects (Di Benedetto et al., eds.)*, Balkema, pp. 59-123.

FHWA. 2001. Mechanically stabilized earth walls and reinforced soil slopes design and construction guidelines, *Federal Highway Administration (FHWA), NHI Course No. 132042, (Elias, V., Christopher, B.R. and Berg, R.R.)*: 73, 114-116. Washington DC., USA.

Greenwood, J.H., Jones, C.J.F.P. and Tatsuoka, F. (2001). Residual strength and its application to design of reinforced soil in seismic areas, *Proc. of IS Kyushu (Ochia et al. eds.)* 1: 37-42. Balkema.

Hirai, T. and Yatsu, A. (2000). "Evaluation method about tensile strength of geogrid to use for dynamic design", *Journal of Geosynthetics Engineering, IGS Japan Chapter*, 15: 205-214 (in Japanese).

Hirakawa, D., Kongkitkul, W., Tatsuoka, F. and Uchimura, T. (2003). "Time-dependent stress-strain behaviour due to viscous properties of geogrid reinforcement", *Geosynthetics International*, 10(6): 176-199.